AIAA JOURNAL
Vol. 48, No. 2, February 2010

Vortex Shedding and Noise Radiation from a Slat Trailing Edge

Sanehiro Makiya,* Ayumu Inasawa,† and Masahito Asai‡
Tokyo Metropolitan University, Tokyo 191-0065, Japan

DOI: 10.2514/1.45777

Vortex shedding and the associated noise radiation from a trailing edge were experimentally investigated for a leading-edge slat of a multi-element airfoil at stowed chord Reynolds number $Re < 5.9 \times 10^5$. A particular focus was on the competition between the instability of the slat boundary layer excited by acoustic feedback and the absolute instability of the wake. Periodic vortex shedding was observed to occur from the slat trailing edge at the Reynolds numbers examined. For $Re < 1.9 \times 10^5$, the vortex shedding is governed by the absolute instability of the laminar wake of the slat without any distinct tonal noise radiation. For $Re > 2.1 \times 10^5$, however, acoustic feedback becomes pronounced between the trailing-edge noise and the boundary-layer instability waves on the suction surface, so that multiple spectral peaks appear both in the velocity fluctuations and sound pressure. At and around the Reynolds number for the first appearance of tonal noise, $Re = 1.9 \times 10^5$, both of the instability modes coexist. Beyond $Re = 2.1 \times 10^5$, the boundary-layer instability waves excited by the acoustic feedback evolve into high-intensity vortices before reaching the trailing edge and suppress the absolute instability of the wake through diminishing the reversed-flow region in the wake.

Nomenclature

c	=	chord of stowed wing, mm
c_s	=	slat chord, mm
f_n	=	discrete-tone frequency, Hz
Re	=	Reynolds number based on the stowed wing chord
Re_s	=	Reynolds number based on the slat chord
s	=	spanwise length of wing, mm
U	=	mean velocity in the x direction, m/s
U_∞	=	freestream velocity, m/s
u	=	velocity fluctuation in the x direction, m/s
$u_{\rm rms}$	=	root-mean-square value of u, m/s
u_0	=	velocity fluctuation of dominant discrete-tone frequency, m/s
$u_{0,\rm rms}$	=	root-mean-square value of u_0, m/s
$u_{0,{\rm rms},m}$	=	y maximum of $u_{0,\rm rms}$, m/s
x, y, z	=	coordinate system
y_w	=	y coordinate measured from the main-element surface
α	=	angle of attack, deg
δ_g	=	slat gap, mm
δ_o	=	slat overhang, mm
ν	=	kinematic viscosity, m^2/s
θ_0	=	phase of u_0, deg
ω	=	spanwise vorticity component, s^{-1}

I. Introduction

THE leading-edge slat is a high-lift device widely used with a rear flap to suppress the stall of an airfoil at high angles of attack. Many experimental and computational studies have been conducted on the aerodynamic characteristics of multi-element airfoil with high-lift devices. Although the slat realizes high-lift performance, it gives rise to additional airframe noise, which is a serious problem in advanced aircraft design. In fact, a slat generating noise is known to be a significant contributor to airframe noise during the takeoff and landing phases, and its reduction is one of the most important and challenging technologies for the aircraft development. Many studies on the slat generating noise have been conducted both experimentally [1,2] and numerically [3–7] by using a scale model at Reynolds numbers lower than that of actual aircraft, and the results indicated that the narrowband high-frequency noise generated around the slat trailing edge was dominant, although broadband low- and midfrequency noise components (probably) originating in the slat cove were found to be more significant at higher Reynolds numbers for the full-scale model [8]. The present study focuses on the mechanism of generating narrowband trailing-edge noise observed at lower Reynolds numbers, such as in the case of scale-model experiments.

On the noise generation at a trailing edge of a single-element airfoil, Paterson et al. [9] first conducted a detailed experiment for a NACA0012 airfoil and showed that the dominant tone frequency increased in proportion to $U_\infty^{1.5}$, where U_∞ is freestream velocity. In addition, they found the so-called ladder-type variations in the tone frequency; in other words, the frequency varied as a piecewise-continuous function of the freestream velocity, with each rung proportional to $U_\infty^{0.8}$. Arbey and Bataille [10] examined the mechanism of discrete tones observed by Paterson et al. [9] and proposed a feedback-loop model originally suggested by Tam [11] and Fink [12], in which the generation of discrete tones was accounted for by the feedback-loop mechanism between the boundary-layer instability waves (i.e., Tollmien–Schlichting waves) originating at the maximum velocity point of the airfoil surface and acoustic waves generated by the diffraction of instability waves at the trailing edge. Nash et al. [13] also conducted a careful experiment on the tone generation mechanism and showed that the discrete-tone frequency was in good agreement with the frequency of the most amplified instability wave predicted from the velocity profiles of the pressure-surface boundary layer by McAlpine et al. [14]. Desquesnes et al. [15] numerically examined the generation mechanism of the trailing-edge noise of an airfoil to support the feedback-loop mechanism.

On the other hand, when the airfoil wake includes a reversed-flow region, the nature of its absolute instability can lead to a global instability, causing self-sustained wake oscillations; see the review by Huerre and Monkewitz [16] for the absolute and global instabilities. The absolute instability exhibits very sharp frequency selectivity of the resulting wake oscillation, and so there is a possibility of generating discrete tonal noise. Sandberg et al. [17] numerically studied the tonal noise generation from NACA symmetric airfoils of different thicknesses with zero angle of attack at the Reynolds number of 5×10^4. Through exciting the

Received 1 June 2009; revision received 20 October 2009; accepted for publication 25 October 2009.

*Graduate Student, Department of Aerospace Engineering, 6-6 Asahigaoka, Hino.
†Assistant Professor, Department of Aerospace Engineering, 6-6 Asahigaoka, Hino.
‡Professor, Department of Aerospace Engineering, 6-6 Asahigaoka, Hino. Senior Member AIAA.

Tollmien–Schlichting waves in the boundary layer on the upper surface of the airfoil, they showed that the wake instability rather than the boundary-layer instability governed the tonal noise generation for the NACA0012 airfoil, whereas the latter instability was dominant for the NACA0008 airfoil. It was also shown that the absolute instability occurred in the separation bubbles formed on the suction surface when the NACA0012 airfoil was set at an angle of attack of 5° for the same low Reynolds number [18].

For the case of leading-edge slat, the boundary layer on the pressure surface decisively differs from a single-element airfoil because of the existence of a cove region in which transition to turbulence occurs at relatively low Reynolds numbers. On the suction surface of the slat, on the other hand, when the slat position is adjusted properly to generate the highest lift, a strong favorable pressure gradient may stabilize the boundary layer and thus delay the transition. A recent large eddy simulation (LES) by Imamura et al. [7] on the flow around a multi-element airfoil with an actual deployed configuration of high-lift devices indicated that the boundary layer on the suction surface of the slat remained laminar even at a Reynolds number of 1.8×10^6. Khorrami et al. [3] examined flow and acoustic fields around a slat on the basis of the unsteady Reynolds-averaged Navier–Stokes equation and pointed out that the noise generation at a slat trailing edge was attributed to the vortex shedding due to absolute instability of the wake rather than the feedback-loop mechanism at the Reynolds number of 7.2×10^6, although the flow over the suction surface was assumed to be fully turbulent in their computation. Olson et al. [1,2] experimentally studied slat noise generation for various slat configurations at Reynolds numbers below 10^6, showing that the generation mechanism of slat noise was highly dependent on the slat position, especially the slat deflection angle. Their flow visualization also showed that vortex roll-up occurred on the suction surface near the slat trailing edge at low deflection angles when tonal noise was generated.

Thus, in laboratory experiments and direct numerical simulations (or LES) in which the Reynolds numbers are not as high as those of actual commercial aircraft, both the convective boundary-layer instability and the absolute wake instability may occur, depending on the flow conditions. It is thus important to examine competition between growing modes or possible interactions of disturbances resulting from those instabilities to clarify the flow physics associated with the slat trailing-edge noise, and this is the main objective in the present experimental study.

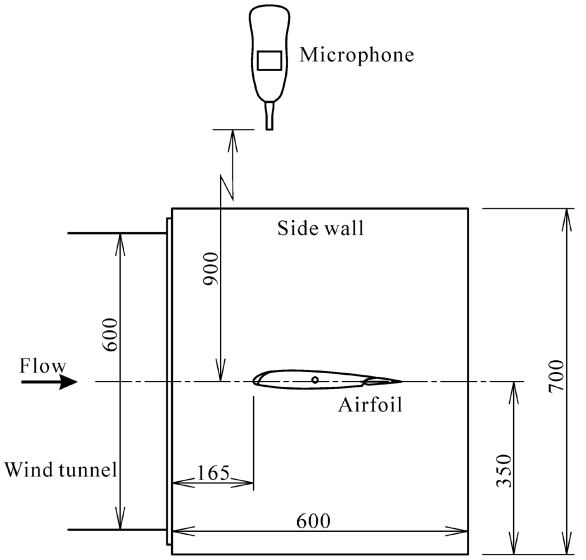

Fig. 1 Schematic of the test section (dimensions in millimeters).

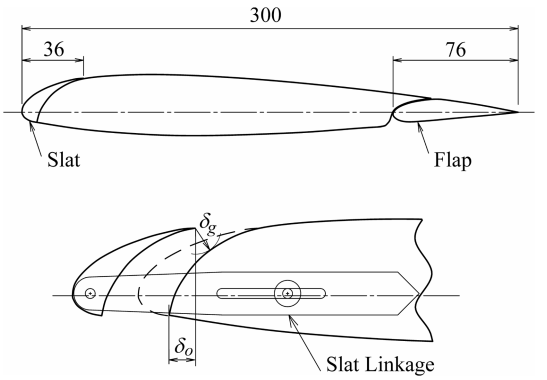

Fig. 2 Configuration of three-element wing model (dimensions in millimeters).

II. Experimental Setup and Procedure

The experiment was conducted in an open-jet type wind tunnel with an exit cross section of 600 mm (height) by 300 mm (span). The wind tunnel has three damping screens spanning the diffuser, five damping screens, and a honeycomb in the settling chamber of 1200×1200 mm in the cross section. The area ratio of the contraction to the test section is 9. The experimental setup is illustrated in Fig. 1. Two Plexiglas sidewalls maintain the two-dimensionality of the main stream in the test section, though the upper and lower areas are opened. A three-element wing model is set between the sidewalls. The configuration of the wing model is illustrated in Fig. 2. The stowed wing consists of a NACA23012 airfoil section, and its chord c and span s are 300 and 282 mm, respectively. The slat is fixed with the main wing by using a linkage. The slat chord c_s is 36 mm; its airfoil section is also illustrated in Fig. 2. Here, the trailing edge of the slat is dull, with a thickness of 0.5 mm. The gap and overhang are denoted as δ_g and δ_o, respectively. In the present experiment, the wing is unflapped and the slat deflection angle is set at 0°, although the slat and flap are deflected in actual high-lift systems (about 30° deflection is typically employed). In this setting, a small separation bubble may appear on the slat suction surface, due to an adverse pressure gradient in the downstream region, which promotes transition through vortex roll-up of the separated shear layer, as observed at small deflection angles in the experiments by Olson et al. [2]. This enabled us to investigate the boundary-layer instability and the wake instability associated with the noise generation mechanism of the slat trailing edge as well as interactions of the vortices resulting from those instabilities. As for the coordinate system, x, y, and z denote the horizontal (oncoming flow direction), vertical, and spanwise directions, respectively. The origin is located at the spanwise center of the slat trailing edge. As will be shown later, the direction of the mean flow is almost parallel to the x direction around the slat trailing edge in the present model configuration.

A constant-temperature hot-wire anemometer is used to measure time-mean and fluctuation velocities U and u. The sensitive length of the hot-wire sensor, a tungsten wire of 5 mm in diameter, is 1 mm. The hot-wire probe can be traversed in the x, y, and z directions. The hot-wire data are stored in a personal computer through A/D conversion. A particle image velocimetry (PIV) system (Dantec), which consists of a double-pulsed Nd:Yag laser and a charge-coupled-device camera of 1280×1024 pixels, is also used to obtain instantaneous velocity fields. In the PIV measurements, the flow is seeded at the wind-tunnel inlet using a smoke generator. To measure aerodynamic noise, a high-precision microphone (RION NL-22, frequency range of 20–8000 Hz, dynamic range of 38–130 dB) is set 900 mm above the slat trailing edge, as shown in Fig. 1. Flow visualization is also done by means of the smoke-wire technique. Two smoke-wires are stretched in the vertical and spanwise directions and still camera shots are taken with stroboscopic light.

The experiment was conducted at freestream velocities U_∞ up to 28 m/s. The Reynolds number based on the stowed chord, Re ($U_\infty c/\nu$), is 5.9×10^5 at $U_\infty = 28$ m/s: The corresponding slat Reynolds number Re_s ($U_\infty c_s/\nu$) is 7.0×10^4. Here, n is the kinematic viscosity. The background freestream turbulence measured at the nozzle exit is less than 0.1% of U_∞ in terms of the rms value of

the streamwise velocity fluctuations u_{rms}. The wind tunnel was not specifically designed for low-noise measurement, and so the overall sound-pressure level (SPL) is 65 dB at $U_\infty = 10$ m/s and 83 dB at $U_\infty = 24$ m/s. However, most of the spectral components are below 1 kHz, lower than that of the generated trailing-edge noise, and the SPL above 1 kHz is about 50 dB at $U_\infty = 10$ m/s and 70 dB at $U_\infty = 24$ m/s. The frequency of the fan blade noise is 190 Hz at $U_\infty = 24$ m/s, much lower than that of the slat trailing-edge noise. Thus, spectral components of noise generated from the slat can be distinguished in the present experimental conditions, as will be shown later, even though the SPL of the total background noise is not sufficiently low.

III. Results and Discussion

In the case of a stowed configuration, the leading-edge stall occurs at angles of attack α higher than 18°, as shown in Figs. 3a and 3b, which visualize flows past the stowed airfoil at $\alpha = 18$ and 20°, respectively, at $U_\infty = 4$ m/s ($Re = 8.4 \times 10^4$). When the slat is adjusted properly, the stall is completely suppressed, as shown in Fig. 3c, which visualizes the flow past the slotted airfoil with $\delta_g/c = 0.014$ and $\delta_o/c = 0.054$ at $\alpha = 20°$. Figures 4a and 4b show close-up pictures of the flow around the slat, corresponding to Fig. 3c. In the side-view picture (Fig. 4a), we see periodic vortex shedding from the trailing edge of the slat. A separation bubble in the cove region is also visualized. The shear layer on the separation bubble remains laminar without noticeable development of Kelvin–Helmholtz instability, owing to the low Reynolds number. Figure 4b displays a top-view picture showing that the vortex shedding is almost two-dimensional. In the following paragraphs, the flowfield and tonal noise generation

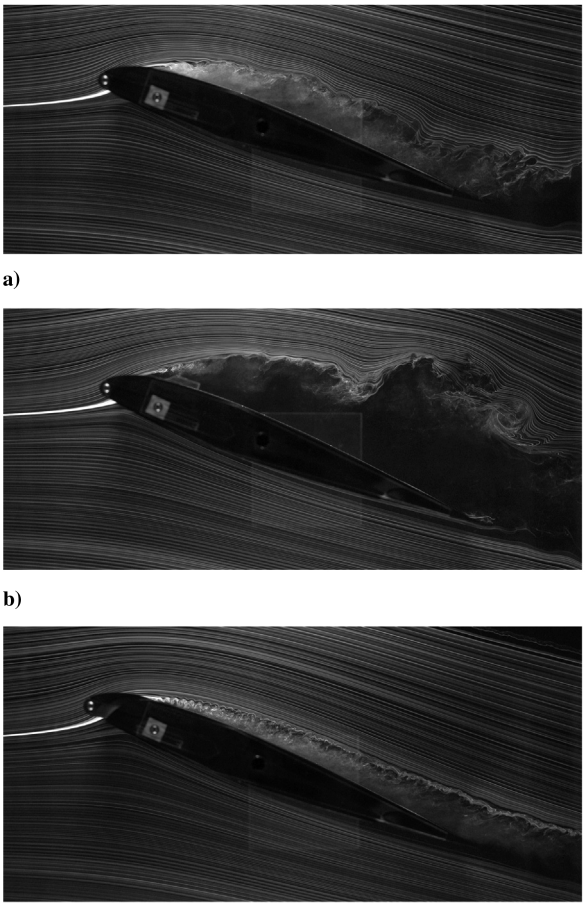

Fig. 3 Visualization of the flow past a NACA23012 airfoil at $Re = 8.2 \times 10^4$ ($U_\infty = 4$ m/s): a) stowed airfoil at $\alpha = 18°$, b) stowed airfoil at $\alpha = 20°$, and c) airfoil with slat at $\alpha = 20°$ ($\delta_g/c = 0.014$ and $\delta_o/c = 0.054$).

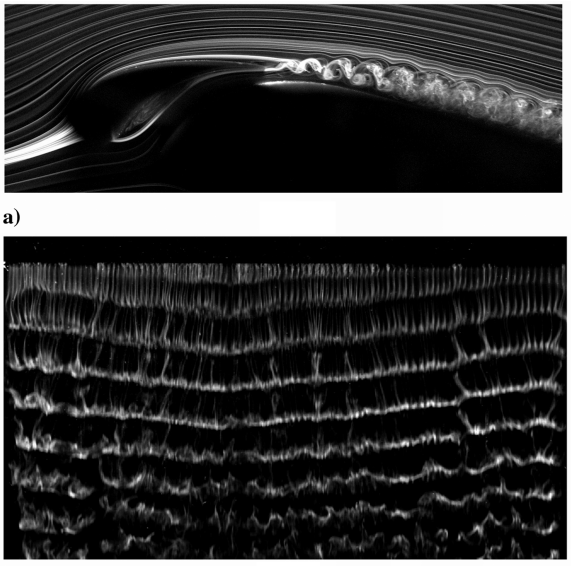

Fig. 4 Visualization of the flow around the slat at $Re = 8.2 \times 10^4$ ($U_\infty = 4$ m/s, $\alpha = 20°$, $\delta_g/c = 0.014$ and $\delta_o/c = 0.054$): a) side view and b) top view.

of the slat trailing edge are examined in detail for the case of slat position with $\delta_g/c = 0.014$ and $\delta_o/c = 0.054$ at $\alpha = 20°$.

Figure 5a shows the isovelocity contours of the mean velocity U in the x–y plane around the slat trailing edge at $U_\infty = 4$ m/s. The velocity data were obtained by PIV, because deep insertion of a hot-wire probe into the near-wake region of the slat can significantly influence the slot flow between the slat and main wing element. A reversed-flow region develops from a location slightly upstream of the trailing edge and extends at least to $x = 2$ mm. The maximum value of the reversed-flow velocity is more than 0.1 U_∞ at and around $x = 1$ mm. Figure 5b displays the y distributions of the time-mean velocity U at three locations: $x = 1.0$, 1.8, and 2.6 mm. Here, note

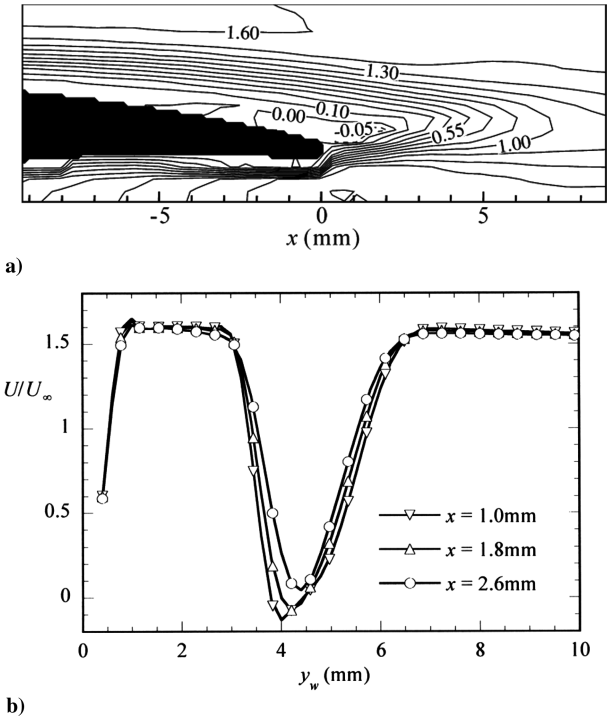

Fig. 5 Mean velocity distributions around the slat trailing edge at $Re = 8.2 \times 10^4$ ($U_\infty = 4$ m/s): a) isovelocity contours and b) velocity profiles in the near wake.

that y_w is measured from the surface of the main element. Both the flows passing the upper (suction side) and lower (pressure side) surfaces of the slat accelerate to the velocity of 1.5 U_∞, although the upper-surface shear layer is thicker than the lower-surface shear layer. In the present configuration, the slat wake seems to be that of an isolated airfoil set in a uniform flow at small angles of attack. Note that the velocity distribution in the slat wake highly depends on the high-lift configuration, and the flow velocity in the slot between the slat and main wing body is about 2.3–3 times the freestream velocity for actual high-lift operations. It is also important to mention that the boundary-layer transition did not occur on either the upper (suction) or lower (pressure) surfaces of the slat at this low freestream velocity. The velocity distribution with the reversed-flow velocity has the nature of absolute instability, which is a prerequisite for the onset of global instability leading to self-sustained periodic wake oscillations (see Huerre and Monkewitz [16]). The wake instability will be discussed again later.

Similar periodic vortex shedding is observed even when the freestream velocity is increased. The power spectra of the velocity fluctuations measured by a hot wire are shown in Figs. 6a, 6c, and 6e, and the SPL measured using a microphone (set above the slat) is shown in Figs. 6b, 6d, and 6f at the freestream velocities of $U_\infty = 9$, 11, and 12 m/s. Here, the spectra of background SPL are also illustrated by broken lines in Figs. 6d and 6f. For the velocity measurements, the hot-wire sensor is placed slightly outside the slat wake at $(x, y) = (10\ \text{mm}, 3\ \text{mm})$ to avoid possible influences on the flow around the slat. At $U_\infty = 9$ m/s, we see no prominent spectral peaks corresponding to the vortex shedding in the SPL spectrum (Fig. 6b). Significantly, the acoustic dipole due to diffraction of vortex-induced sound is weak in this case, not only because the flow Mach number is very low but also because vortex formation occurs at a location not close to the trailing edge.

It is after the freestream velocity exceeds $U_\infty = 10$ m/s that prominent discrete spectra appear at the shedding frequencies in SPL, as shown in Figs. 6c and 6d and Figs. 6e and 6f. In fact, Fig. 7 plots the SPL of the discrete tones against the freestream velocity to show the critical velocity for the onset of discrete tones. The SPL increases steeply around $U_\infty = 10$ m/s. Here, the slat Reynolds number Re_s is only 2.5×10^4 at $U_\infty = 10$ m/s.

The frequency variations of vortex shedding and discrete tones are examined next. When the acoustic noise is generated beyond $U_\infty = 10$ m/s, the spectra exhibit multiple sharp peaks, as shown in

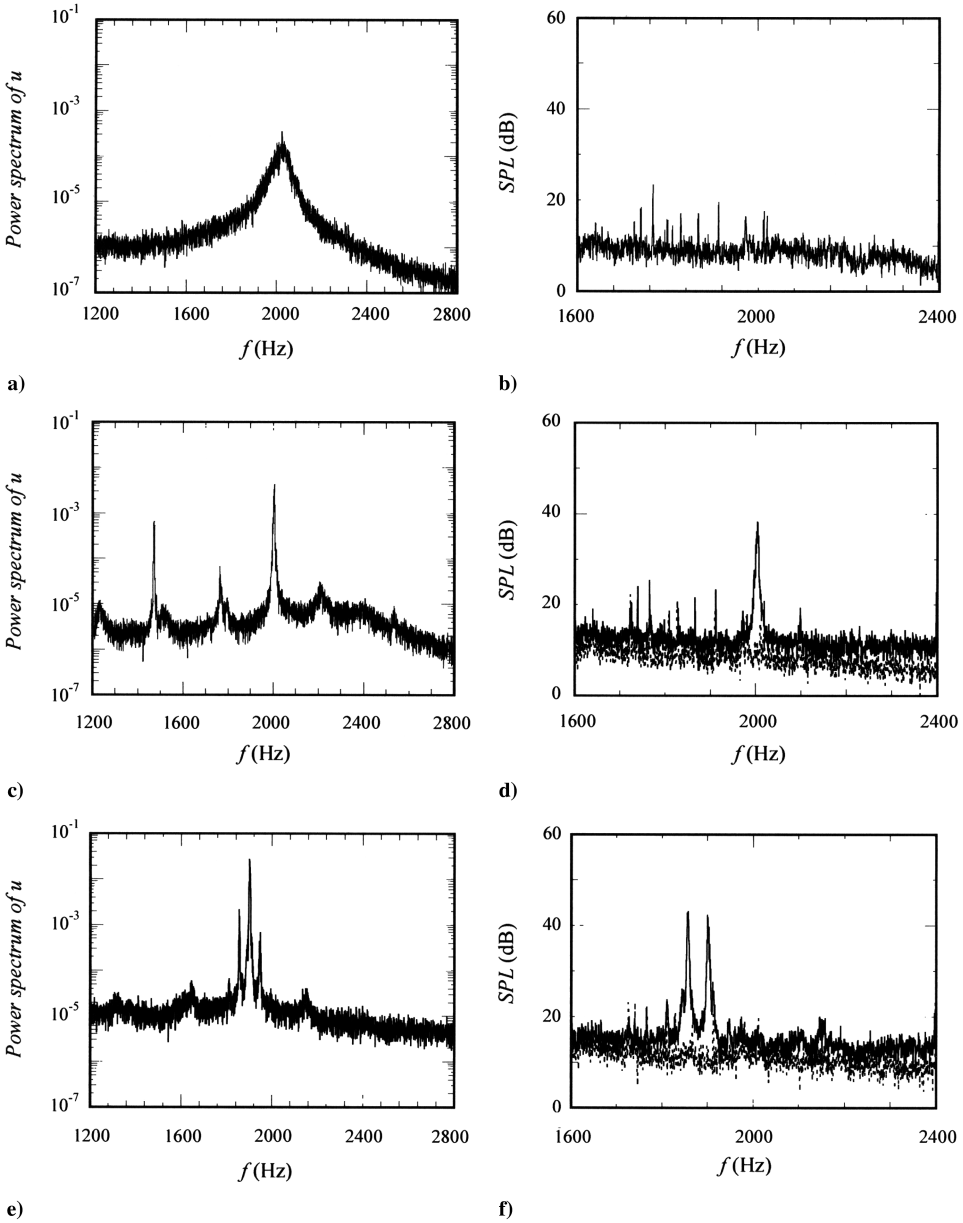

Fig. 6 Power spectra of u fluctuations and SPL: a–b) $Re = 1.9 \times 10^5$ ($U_\infty = 9$ m/s), c–d) $Re = 2.3 \times 10^5$ ($U_\infty = 11$ m/s), and e–f) $Re = 2.5 \times 10^5$ ($U_\infty = 12$ m/s); broken lines represent the spectra of background noise.

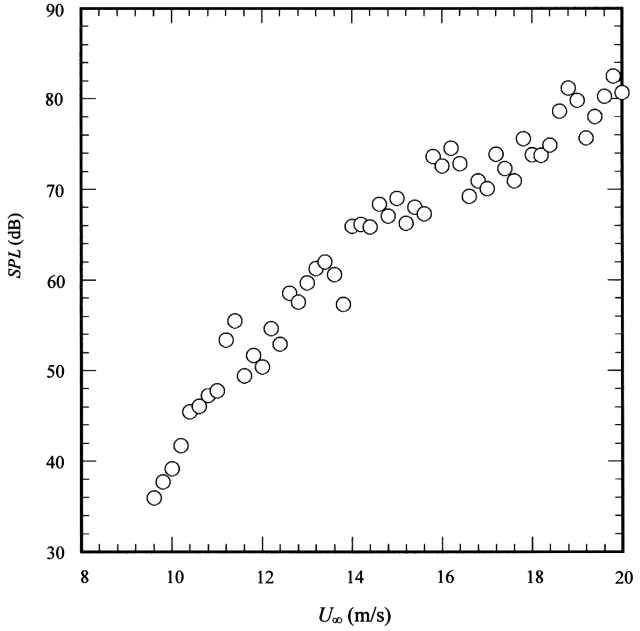

Fig. 7 SPL of discrete tones vs freestream velocity U_∞.

Fig. 6. We obtain the frequencies of such discrete spectra f_n for each freestream velocity U_∞. Figures 8a and 8b illustrate the frequency variations of the discrete spectra of velocity fluctuation and sound, respectively. Here, only discrete tones corresponding to the discrete spectra of velocity fluctuations are plotted in Fig. 8b. Up to $U_\infty =$ 9 m/s ($Re = 1.9 \times 10^5$), where there is no appreciable noise generation (see Fig. 7), a single dominant frequency is detected for the velocity spectra measured in the wake at each freestream velocity, and it increases almost linearly proportional to U_∞ (except for the small freestream velocities below 5 m/s) in Fig. 8a. When the Strouhal number is defined on the basis of the wake width instead of the slat chord, it is about 0.14 for $U_\infty = 5$–9 m/s ($Re = 1.1 \times 10^5$ to 1.9×10^5). The Reynolds number dependency of the Strouhal number is similar to that of the von Kármán vortex shedding of a circular-cylinder wake at low Reynolds numbers (see Williamson [19]). A drastic change occurs in the dominant frequency when U_∞ approaches 10 m/s. For $U_\infty \geq 9.6$ m/s, multiple spectral peaks appear and their frequencies exhibit ladder-type variations, with each rung proportional to $U_\infty^{0.85}$. Correspondingly, discrete tones for which the frequency varies with the same ladder-type variations appear for $U_\infty \geq 9.8$ m/s (Fig. 8b). These ladder-type frequency variations are similar to those found in the past experiments on the discrete-tone generation in a single-element airfoil at small angles of attack by Paterson et al. [9], Arbey and Bataille [10], and Nash et al. [13]. The result suggests the change in the mechanism of vortex shedding around $U_\infty = 10$ m/s ($Re = 2.1 \times 10^5$): that is, the change from the absolute instability of the slat near wake to a feedback-loop mechanism between the boundary-layer instability upstream of the slat trailing edge and vortex-induced trailing-edge noise. Figures 9a–9d compare the power spectra of velocity fluctuations at $U_\infty = 9.2$, 9.6, 10, and 11 m/s, respectively. Interestingly, we can see both kinds of spectral peaks in the power spectra of velocity fluctuations in the transitional velocity range at $U_\infty = 9.6$ and 10 m/s. One is a spectrum corresponding to the absolute instability mode (which was observed in the case of $U_\infty = 9.2$ m/s) and the other corresponds to the sharp discrete tones. These spectra strongly suggest that the boundary-layer instability modes excited by the acoustic feedback and the absolute instability mode of the wake coexist and their competition occurs around $U_\infty = 9.6$–10 m/s. With an increase in the freestream velocity, the acoustic feedback is intensified, owing to generated sound being strengthened, and the boundary-layer instability waves can evolve into strong vortices before reaching the trailing edge. Beyond $U_\infty = 10$ m/s, such high-intensity vortices suppress the growth of the absolute instability mode through alternating the near-wake structure. This will be discussed again later on the basis of the velocity distribution around the slat trailing edge.

To clarify the differences in the vortex shedding at the trailing edge with and without radiation of the strong discrete tone, we examined the instantaneous flow structure near the slat trailing edge in detail. Figures 10a and 10b show instantaneous vorticity distributions in the low-velocity (or low Reynolds number) cases without tonal noise detection at $U_\infty = 4$ and 8 m/s, respectively. These were obtained from PIV data. Development of the von Kármán vortex street is visible in correspondence with the smoke-wire photographs shown in Fig. 3. On the other hand, Fig. 11 displays instantaneous vorticity distributions in the case of discrete-tone generation at $U_\infty = 13$ m/s. Compared with the lower-velocity cases ($U_\infty = 4$ and 8 m/s), we can see the formation of the vortex street much closer to the trailing edge at $U_\infty = 13$ m/s. In particular, the strong vortices for which the maximum vorticity is almost the same as that of wake vortices had already formed on the upper (suction-side) surface slightly upstream of the trailing edge and have developed into a pair of counter-rotating vortices (with opposite sign of vorticity) just downstream of the trailing edge. Such vortex shedding close to the trailing edge may, no doubt, induce the strong acoustic dipole at the slat trailing edge. The trailing-edge noise thus generated propagates upstream and excites the boundary-layer instability waves on the upper surface of the slat through the receptivity process. To ensure this, we examined the development of the velocity fluctuation of the most dominant discrete-tone frequency u_0 along the suction surface of the slat.

Figures 12a and 12b display the streamwise variations of the maximum rms value $u_{0,\mathrm{rms},m}$, i.e., the y maximum of $u_{0,\mathrm{rms}}$, and phase θ_0 of u_0, respectively. Here, the phase θ_0 was measured at the y position, where $u_{0,\mathrm{rms}}$ takes the maximum by using the output of the

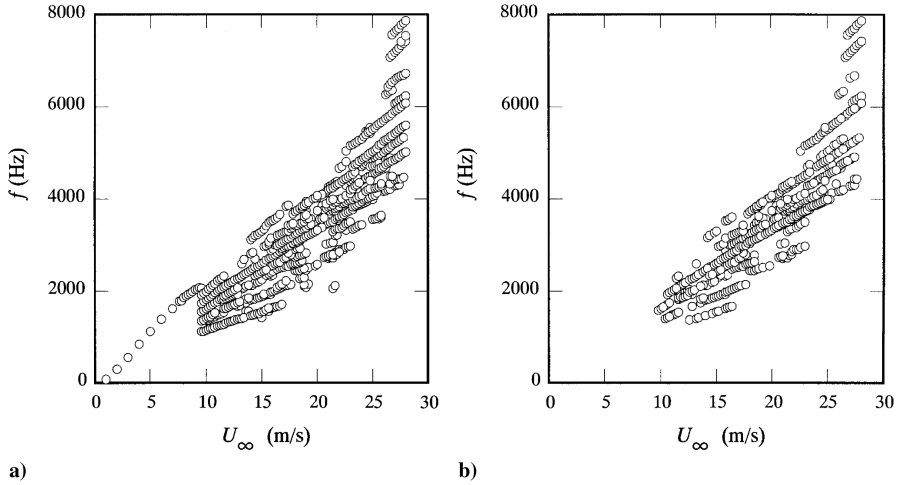

Fig. 8 Frequencies of discrete spectra of a) velocity fluctuation and b) sound.

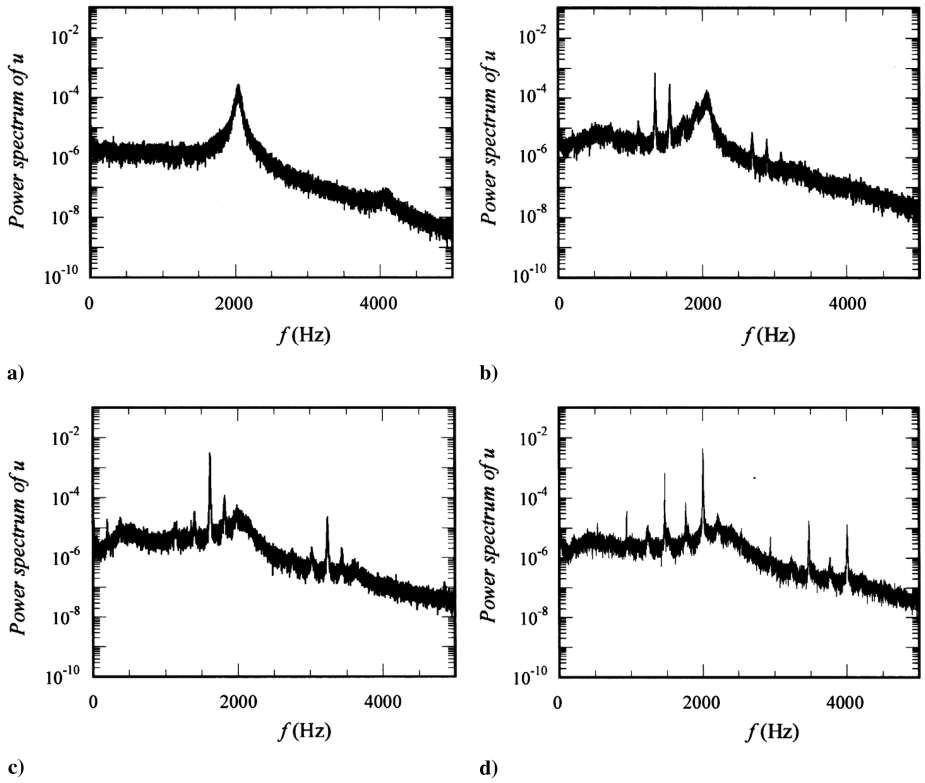

Fig. 9 Power spectra of u fluctuations immediately downstream of the trailing edge: a) $Re = 1.9 \times 10^5$ ($U_\infty = 9.2$ m/s), b) $Re = 2.0 \times 10^5$ ($U_\infty = 9.6$ m/s), c) $Re = 2.1 \times 10^5$ ($U_\infty = 10$ m/s), and d) $Re = 2.3 \times 10^5$ ($U_\infty = 11$ m/s).

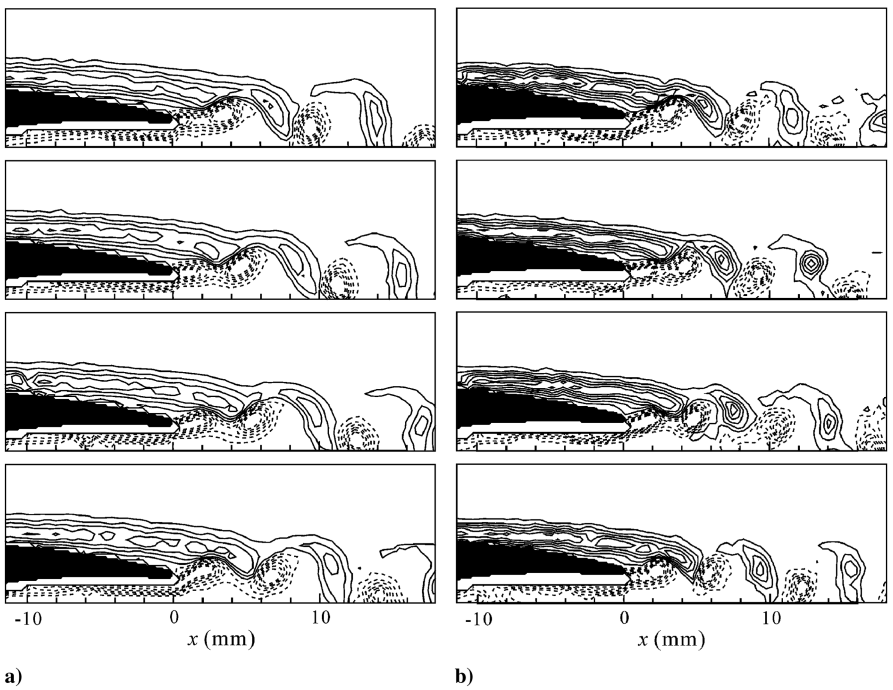

Fig. 10 Instantaneous vorticity field near the trailing edge. Contour lines range from $\omega c_s/U_\infty = -55$ to 55 with intervals of 10. Solid and broken lines represent negative and positive values, respectively: a) $Re = 8.2 \times 10^4$ ($U_\infty = 4$ m/s) and b) $Re = 1.7 \times 10^5$ ($U_\infty = 8$ m/s).

microphone (fixed at a location) as the reference signal. The phase is nearly constant for $x < -10$ mm (upstream of the separation point), indicating that the acoustic component is still dominant there, whereas θ_0 varies linearly with x for $x > -10$ mm, showing the development of an instability wave there, and its streamwise wavelength is obtained to be about 4 mm as a streamwise distance over which the phase changes by 2π. Correspondingly, the disturbance undergoes exponential growth downstream from $x = -10$ mm. The acoustic disturbance caused by the shed vortices is intensified at the trailing edge due to the diffraction and is radiated upstream along the slat surface. Such an acoustic disturbance can, no doubt, excite the boundary-layer instability through the receptivity process [20]. The boundary-layer instability waves undergo sufficient amplification due to the inflectional instability under the adverse pressure gradient before reaching the trailing edge and evolve into strong vortices leading to the von Kármán vortex street in

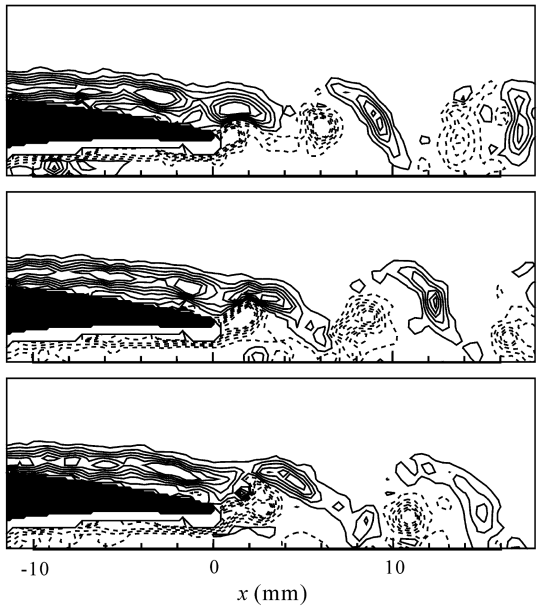

Fig. 11 Instantaneous vorticity field near the trailing edge at $Re = 2.7 \times 10^5$ ($U_\infty = 13$ m/s). Contour lines range from $\omega c_s/U_\infty = -55$ to 55 with intervals of 10. Solid and broken lines represent negative and positive values, respectively.

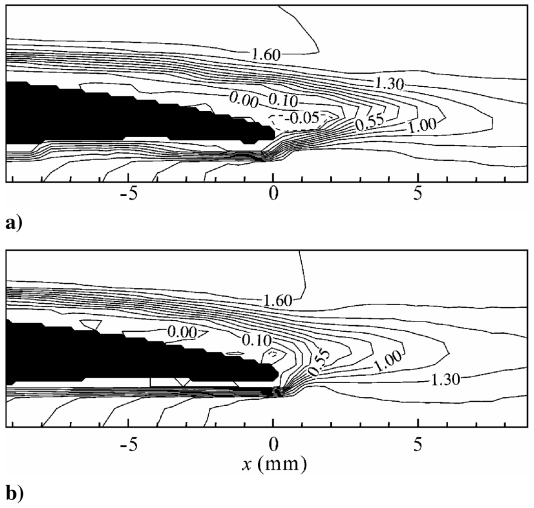

Fig. 13 Contours of U/U_∞ around the trailing edge: a) $Re = 1.7 \times 10^5$ ($U_\infty = 8$ m/s) and b) $Re = 2.7 \times 10^5$ ($U_\infty = 13$ m/s).

the wake, as shown in Fig. 11. Thus, the results strongly suggest that a feedback-loop mechanism sets in when the velocity (or the Reynolds number) exceeds the critical value.

Finally, we consider why the absolute instability is suppressed for $U_\infty > 10$ m/s again by comparing the near-wake structures below and above the critical freestream velocity for the occurrence of the prominent discrete tone. Figure 13 compares the isovelocity contours of the mean streamwise velocity component U around the slat trailing edge at $U_\infty = 8$ and 13 m/s, below and above the critical speed for the discrete-tone generation, respectively. In the flow at $U_\infty = 8$ m/s, a reversed-flow region is distinctly visible, similar to the flow at $U_\infty = 4$ m/s (see Fig. 5a). For the case of tone generation at $U_\infty = 13$ m/s, on the other hand, the reversed-flow region almost disappears in the wake, implying that the nature of absolute instability becomes weak or disappears.

IV. Conclusions

To better understand the mechanism of trailing-edge noise generation of a leading-edge slat, vortex shedding and associated noise generation were experimentally investigated at the stowed chord Reynolds numbers $Re < 5.9 \times 10^5$, where the boundary layer on the suction side of the slat is laminar or transitional. A particular focus was on the interactions of vortices resulting from the boundary-layer instability on the slat surface and the wake instability. No deflection angle was employed to examine such interactions. The periodic vortex shedding from the slat was observed to occur over the Reynolds numbers examined in the present wing configuration. For low freestream conditions below 10 m/s, where $Re < 2.1 \times 10^5$, the vortex shedding is governed by the global (absolute) instability of the laminar wake of the slat. No distinct tonal noise was detected because the low Mach number of the flow and vortex formation at some distance from the slat trailing edge prevented the acoustic dipole from being sufficiently strong. For $Re > 2.1 \times 10^5$, on the other hand, spectral peaks appeared distinctly both in the velocity fluctuations and sound pressure. The frequencies of the velocity fluctuations and dominant discrete tones exhibited the so-called ladder-type variations, with each rung proportional to $U_\infty^{0.85}$. The variations are similar to those found in the past experiments [9,10,13] on the trailing-edge noise for the case of single-element airfoil at small angles of attack. The feedback-loop mechanism between the generated sound and instability waves excited in the boundary layer on the slat suction-surface was found to be responsible for the tonal noise generation, although in the case of the single-element airfoil, the feedback-loop mechanism operates on the pressure surface for a wide range of Reynolds numbers. When the feedback loop sets in, the boundary-layer instability waves are sufficiently amplified under adverse pressure gradient and develop into high-intensity vortices

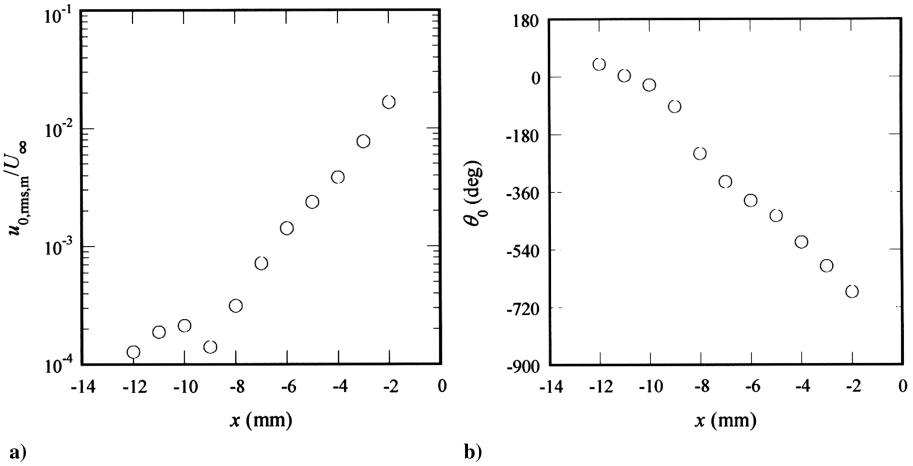

Fig. 12 Streamwise variations of root-mean-square value $u_{0,\mathrm{rms},m}$ and phase θ_0 of u_0 of dominant discrete-tone frequency on the upper airfoil surface near the trailing edge at $Re = 2.7 \times 10^5$ ($U_\infty = 13$ m/s).

before reaching the trailing edge, which generates a strong acoustic (dipole) source at the slat trailing edge by diffraction of the vortex-induced fluctuations. It was also found that the boundary-layer instability modes excited by the acoustic feedback and the absolute instability mode of the wake coexist and their competition occurs at Reynolds numbers between $Re = 1.9 \times 10^5$ ($U_\infty = 9.2$ m/s) and 2.1×10^5 ($U_\infty = 10$ m/s). When the freestream velocity exceeds the critical value around $U_\infty = 10$ m/s, the acoustic feedback is intensified so that strong vortices can develop in the slat boundary layer, which suppresses the growth of the absolute instability mode by markedly diminishing the reversed-flow region in the wake.

The present experiment was conducted in the absence of deflection of the slat and flap as well as at low Reynolds numbers. Therefore, the results might not be directly applicable to high-lift systems of actual aircraft. However, we may safely say that as long as the boundary-layer instability waves can evolve into high-intensity vortices close to the trailing edge, the feedback loop is the key mechanism for generating tonal noise at the trailing edge.

Acknowledgment

This work was supported in part by a grant for scientific research from the Tokyo Metropolitan Government.

References

[1] Olson, S., Flint, O., Nelson, T., and Nelson, R. C., "A Preliminary Investigation into Slat Noise Production Mechanisms in a High-Lift Configuration," AIAA Paper 2000–4508.

[2] Olson, S., Flint, O., Nelson, T., and Nelson, R. C., "Mechanisms of Slat Noise Production in a 2D Multi-Element Airfoil Configuration," AIAA Paper 2001–2156.

[3] Khorrami, M. R., Berkman, M. E., and Choudhari, M., "Unsteady Flow Computations of a Slat with a Blunt Trailing Edge," *AIAA Journal*, Vol. 38, No. 11, 2000, pp. 2050–2058. doi:10.2514/2.892

[4] Khorrami, M. R., Singer, B. A., and Berkman, M. E., "Time-Accurate Simulations and Acoustic Analysis of Slat Free Shear Layer," *AIAA Journal*, Vol. 40, No. 7, 2002, pp. 1284–1291. doi:10.2514/2.1817

[5] Khorrami, M. R., and Choudhari, M. M., "Application of Passive Porous Treatment to Slat Trailing Edge Noise," NASA TM-212416, 2003.

[6] Takeda, K., Zhang, X., and Nelson, P. A., "Computational Aeroacoustic Simulations of Leading-Edge Slat Flow," *Journal of Sound and Vibration*, Vol. 270, No. 3, 2004, pp. 559–572. doi:10.1016/j.jsv.2003.09.046

[7] Imamura, T., Enomoto, S., Yokokawa, Y., and Yamamoto, K., "Three-Dimensional Unsteady Flow Computations Around a Conventional Slat of High-Lift Devices," *AIAA Journal*, Vol. 46, No. 5, 2008, pp. 1045–1053. doi:10.2514/1.25660

[8] Dobrzynski, W., Ewert, R., Pott-Pollenske, M., Herr, M., and Delfs, J., "Research at DLR Towards Airframe Noise Prediction and Reduction," *Aerospace Science and Technology*, Vol. 12, No. 1, 2008, pp. 80–90. doi:10.1016/j.ast.2007.10.014

[9] Paterson, R. W., Vogt, P. G., Fink, M. R., and Munch, C., "Vortex Noise of Isolated Airfoils," *Journal of Aircraft*, Vol. 10, No. 5, 1973, pp. 296–302. doi:10.2514/3.60229

[10] Arbey, H., and Bataille, J., "Noise Generated by Airfoil Profiles Placed in a Uniform Laminar Flow," *Journal of Fluid Mechanics*, Vol. 134, 1983, pp. 33–47. doi:10.1017/S0022112083003201

[11] Tam, C. K. W., "Discrete Tones of Isolated Airfoils," *Journal of the Acoustical Society of America*, Vol. 55, No. 6, 1974, pp. 1173–1177. doi:10.1121/1.1914682

[12] Fink, M. R., "Prediction of Airfoil Tone Frequencies," *Journal of Aircraft*, Vol. 12, No. 2, 1975, pp. 118–120. doi:10.2514/3.44421

[13] Nash, C. E., Lowson, M. V., and McAlpine, A., "Boundary-Layer Instability Noise on Aerofoils," *Journal of Fluid Mechanics*, Vol. 382, 1999, pp. 27–61. doi:10.1017/S002211209800367X

[14] McAlpine, A., Nash, E. C., and Lowson, M. V., "On the Generation of Discrete Frequency Tones by the Flow Around an Aerofoil," *Journal of Sound and Vibration*, Vol. 222, 1999, pp. 753–779. doi:10.1006/jsvi.1998.2085

[15] Desquesnes, G., Terracol, M., and Sagaut, P., "Numerical Investigation of the Tone Noise Mechanism over Laminar Airfoils," *Journal of Fluid Mechanics*, Vol. 591, 2007, pp. 155–182. doi:10.1017/S0022112007007896

[16] Huerre, P., and Monkewitz, P. A., "Local and Global Instabilities in Spatially Developing Flows," *Annual Review of Fluid Mechanics*, Vol. 22, 1990, pp. 473–537. doi:10.1146/annurev.fl.22.010190.002353

[17] Sandberg, R. D., Jones, L. E., Sandham, N. D., and Joseph, P. F., "Direct Numerical Simulations of Tonal Noise Generated by Laminar Flow Past Airfoil," *Journal of Sound and Vibration*, Vol. 320, Nos. 4–5, 2009, pp. 838–858. doi:10.1016/j.jsv.2008.09.003

[18] Jones, L. E., Sandberg, R. D., and Sandham, N. D., "Direct Numerical Simulations of Forced and Unforced Separation Bubbles on an Airfoil at Incidence," *Journal of Fluid Mechanics*, Vol. 602, 2008, pp. 175–207. doi:10.1017/S0022112008000864

[19] Williamson, C. H. K., "Oblique and Parallel Modes of Vortex Shedding in the Wake of a Cylinder," *Journal of Fluid Mechanics*, Vol. 206, 1989, pp. 579–627. doi:10.1017/S0022112089002429

[20] Saric, W., Reed, H. L., and Kerschen, E. J., "Boundary Layer Receptivity to Freestream Disturbances," *Annual Review of Fluid Mechanics*, Vol. 34, 2002, pp. 291–319. doi:10.1146/annurev.fluid.34.082701.161921

F. Coton
Associate Editor